Codoping Er-N to Suppress Self-Compensation Donors for Stable *p*-Type Zinc Oxide

Yifang Ouyang, Zhisen Meng, Xiaoming Mo, Hongmei Chen, Xiaoma Tao, Qing Peng,* and Yong Du*

Stable *p*-type doping of zinc oxide (ZnO) is an unsolved but critical issue for ultraviolet optoelectronic applications despite extensive investigations. Here, an Er-N codoping strategy for defect engineering of ZnO to suppress the self-compensation of the donor-type intrinsic point defects (IPDs) over the acceptor-type ones is proposed. Via first-principles calculations, the influence of nitrogen and erbium concentration on the stability of ZnO is investigated. The complex (Er_{Zn}-mN_O) consisting of multiple substitutional N on O sites and one substitutional Er on Zn site is a crucial stabilizer. With an increase of the concentration of N, the absorption edges redshift to lower energy due to the impurity band broadening in the bandgap. The results suggest that codoping Er-N into the ZnO matrix is a feasible way to manufacture stable *p*-type ZnO.

1. Introduction

The Er-N codopant is stable for zinc oxide (ZnO), suppressing the self-compensation of the donor-type intrinsic point defects (IPDs), with a strong infrared absorption when the N concentration is above 1.389%.

Zinc oxide (ZnO) is one of the most important semiconductors with attractive properties[1–3] and wide applications.[4] However, some vital problems that hinder the further development of ZnO-based optoelectronic devices still remain unsolved; for example, *p*-type doping ZnO with high hole concentration is still unavailable, partially due to the strong self-compensation of the donor-type IPDs over the acceptors in ZnO itself. Therefore, suppressing the self-compensation and improving the solubility of the acceptors is critical to produce stable and reliable *p*-type ZnO, which becomes a highly elevated task and is required by fabrication of different kinds of semiconductor devices. Till now, many doping strategies have been proposed in order to realize *p*-type ZnO. Some groups reported doping strategies by doping Group I or V elements (Li, Na, Ag, N, P, As, etc.) to the ZnO matrix to produce *p*-type ZnO.[5–10] These methods were simple, but the as-produced *p*-type ZnO was not stable due to the strong self-compensation and low solubility of the acceptors. For this reason, Yamamoto and Katayama-Yoshida proposed a strategy by codoping N and Al(Ga) into ZnO to decrease the Madelung energy and ionization energy, and thus enhance the incorporation of the N acceptors.[11] Besides, some theoretical and experimental codoping methods by using N and many other different dopants was also carried out to produce *p*-type ZnO; for example, N codoping with P,[12] Mg,[13] Ag,[14,15] Li,[16–19] B,[20,21] Be,[22]As,[23] etc. Other codoping methods, such as Li-F,[24] Al-As,[25] Ag-S,[26,27] Mg-F,[28] and Li-P[29] were proposed as well.

Indeed, doping (including codoping) is a simple and effective means to improve the electrical and optical properties of ZnO.[30–33] Except for the Group I, III, and/or V elements mentioned above, rare earth (RE)-doped ZnO materials also show great potential for producing optoelectronic devices due to their unique electronic structures. Extensive studies have been carried out for RE-doped ZnO, including Eu,[32] Er,[33,34] Tm,[35] Yb,[36] La,[37] and Nd.[38] Among them, Er is a very promising dopant because the unique intra-4*f* transitions of Er can produce strong emission at 1.54 μm ($^4I_{13/2} \rightarrow {}^4I_{15/2}$),[39] which lies in the minimum loss region of silica-based optical fibers and can be used in future optical telecommunication. Er can inherently inhibit the donor-type IPDs in ZnO and favor the formation of acceptor-type IPDs.[31] However, doping Er into the ZnO lattice alone is not likely to form *p*-type ZnO with high hole concentration due to the low concentration and solubility of the acceptors.

In this paper, a codoping strategy by codoping Er and N into ZnO is proposed to surpass the difficulties as noted above. The crystal structures, formation energies, ionization energies, band structures, and optical properties of the Er-N codoped ZnO are studied via first-principles calculations. Er_{Zn}-mN_O complexes were found to be the main configurations in the Er-N codoped ZnO systems due to their small lattice distortions, formation energies, and ionization energies. Electronic and optical properties of these systems were further analyzed.

Prof. Y. Ouyang, Z. Meng, Dr. X. Mo, Prof. H. Chen, Prof. X. Tao
College of Physical Science and Technology
Guangxi University
Nanning, Guangxi 530004, People's Republic of China
E-mail: taoxiaoma@gxu.edu.cn

Dr. Q. Peng
Department of Nuclear Engineering and Radiological Science
University of Michigan
Ann Arbor, MI 48109, USA
E-mail: qpeng.org@gmail.com

Prof. Y. Du
State Key Laboratory of Powder Metallurgy
Central South University
Changsha, Hunan 410083, People's Republic of China

The ORCID identification number(s) for the author(s) of this article can be found under https://doi.org/10.1002/adts.201800133

DOI: 10.1002/adts.201800133

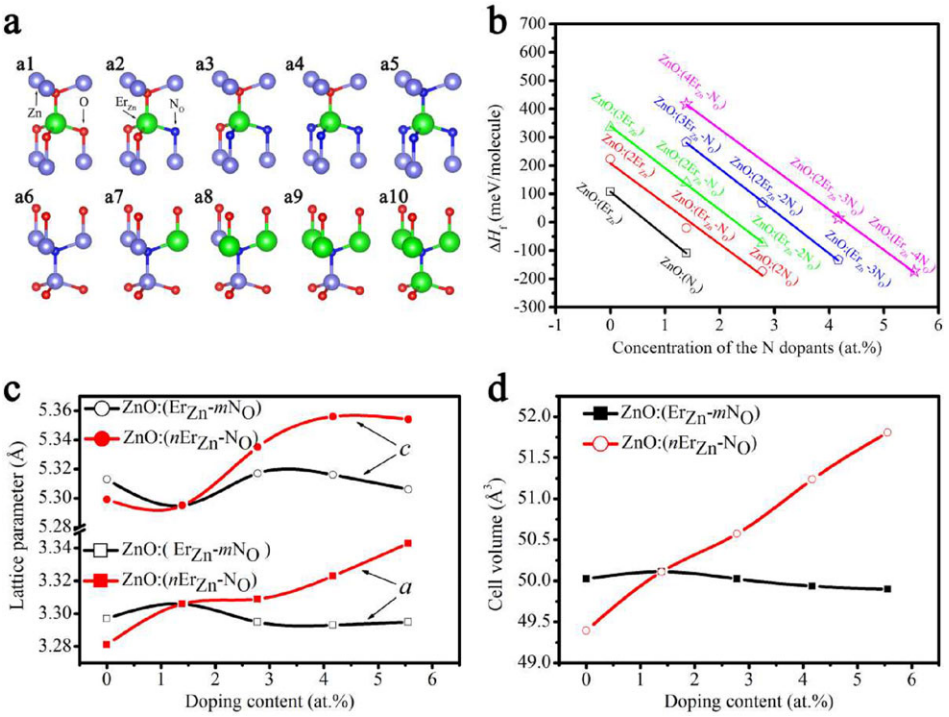

Figure 1. Er-N co-dopants. a) partial view of the models considered: (a1–a5) ZnO:(Er_{Zn}-mN_O) ($m = 0, 1, 2, 3, 4$) and (a6–a10) ZnO:(nEr_{Zn}-N_O) ($n = 0, 1, 2, 3, 4$). (a2) and (a7) are actually the same model observed from different angles. b) Formation enthalpies of per molecule of ZnO:(Er_{Zn}) for different co-doping concentration, the line for guide to variation of N and Er with co-doping concentration. For some total co-doping concentration, the formation enthalpy is lower when the more N dopant. c) Lattice parameters (*a* and *c*) for hexagonal structures, and d) cell volume for the configurations codoped as a function of the Er and N doping concentrations. The lattice constants and cell volume decrease slightly with N doping concentration, while increase with Er doping concentration. The N doping influences much less on the crystal parameters than that of Er doping in the Er-N co-doping systems.

2. Results

2.1. Structures

The view of the part of the configurations of the codopant models considered is illustrated in **Figure 1**(a). Crystal parameters of the Er-N codoping ZnO:(nEr_{Zn}-mN_O) systems were computed with the condition that all the degrees of freedom of the system are free to move. The results of the lattice constants and volumes of these configurations are shown in Figure 1(c) and (d). From the results of ZnO:(Er_{Zn}-mN_O) ($m = 0, 1, 2, 3, 4$) in Figure 1(c), it can be found that with increasing the doping concentration of N c_N, lattice parameter *a* firstly increases a little but decreases when $c_N > 1.389$ at%. The lattice parameter *c* firstly decreases, then increases as $c_N > 1.389$ at%, and decreases again when $c_N > 2.778$ at%. For ZnO:(nEr_{Zn}-N_O) ($n = 0, 1, 2, 3, 4$), parameter *c* behaves similarly as that of ZnO:(Er_{Zn}-mN_O), but parameter *a* is very different because it increases monotonically with increasing the Er concentration. Figure 1(d) shows the change of the cell volume as a function of the doping concentration. The cell volume only decreases slightly with increasing the N concentration. On the contrary, the cell volume increases dramatically with increasing the Er concentration. This could be understood from the fact that the ionic radius of Er^{3+} (0.890 Å) is much bigger than that of Zn^{2+} (0.740 Å), leading to volume expansion for Er doping.[33] Therefore, the doping N influences much less on the crystal parameters than that of doping Er in the Er-N codoping systems.

2.2. Formation Enthalpies

The effect of concentration of Er-N codoping on the formation enthalpies is presented in Figure 1(b). The formation enthalpies vary linearly with the concentration of N for the complexes with same number of total dopants. Two representative codoping complexes [ZnO:(Er_{Zn}-mN_O) ($m = 0, 1, 2, 3, 4$) and ZnO:(nEr_{Zn}-N_O) ($n = 0, 1, 2, 3, 4$)] were used and they corresponded to concentration of the N (Er) dopants of 0, 1.389, 2.778, 4.167, and 5.556 at% for different *m* (*n*), respectively.

2.3. Ionization Energy and Defect Formation Energy

Ionization energies of the defects with different N doping concentration (Figure 4) show that the values of $\varepsilon(0/-1)$ for Er_{Zn}-$3N_O$ and Er_{Zn}-$4N_O$ complexes are 1.008 and 0.244 eV, respectively, while the values of $\varepsilon(-1/-2)$ for Er_{Zn}-$3N_O$ and Er_{Zn}-$4N_O$ complexes are 0.574 and 0.233 eV, respectively. The values of $\varepsilon(0/-1)$ are greater than those of $\varepsilon(-1/-2)$ for the Er_{Zn}-$3N_O$ and Er_{Zn}-$4N_O$ complexes, indicating that the defect charge is directly transformed from neutral to –2. The defect formation energies of ZnO:(Er_{Zn}-mN_O) ($m = 0, 1, 2, 3, 4$) and ZnO:(nEr_{Zn}-N_O) ($n = 0, 1, 2, 3, 4$) are displayed in **Figure 2** as a function of the Fermi level under different chemical potential conditions. The range of the Fermi energy is given by the calculated the valence band maximum (VBM) (0 eV) and conduction band minimum (CBM) (3.412 eV).

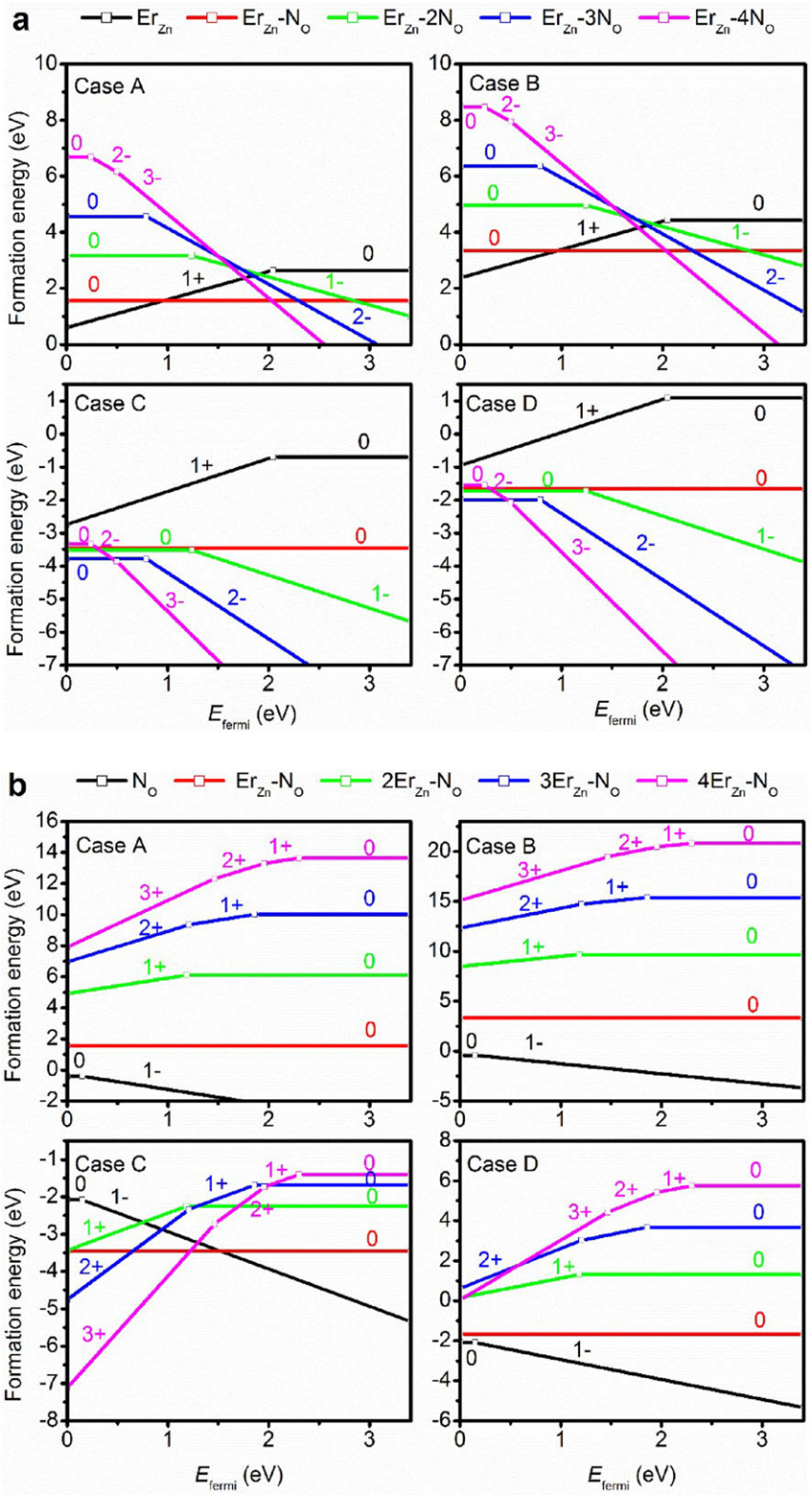

Figure 2. Formation energy versus Fermi level of doping systems for different extreme chemical potential conditions (case A: Zn-rich, Er-rich, case B: Zn-rich Er-poor, case C: Zn-poor, Er-poor, case D: Zn-poor, Er-rich). a) Formation energies of ZnO:(Er_{Zn}-mN_O) ($m = 0, 1, 2, 3, 4$) as a function of the Fermi level for different chemical potential conditions. b) Formation energies of ZnO:(nEr_{Zn}-N_O) ($n = 0, 1, 2, 3, 4$) as a function of the Fermi level for different chemical potential conditions. The defect transition energies became shallower with increasing the N concentration and the nEr_{Zn}-N_O complexes are not as stable as the Er_{Zn}-mN_O complexes.

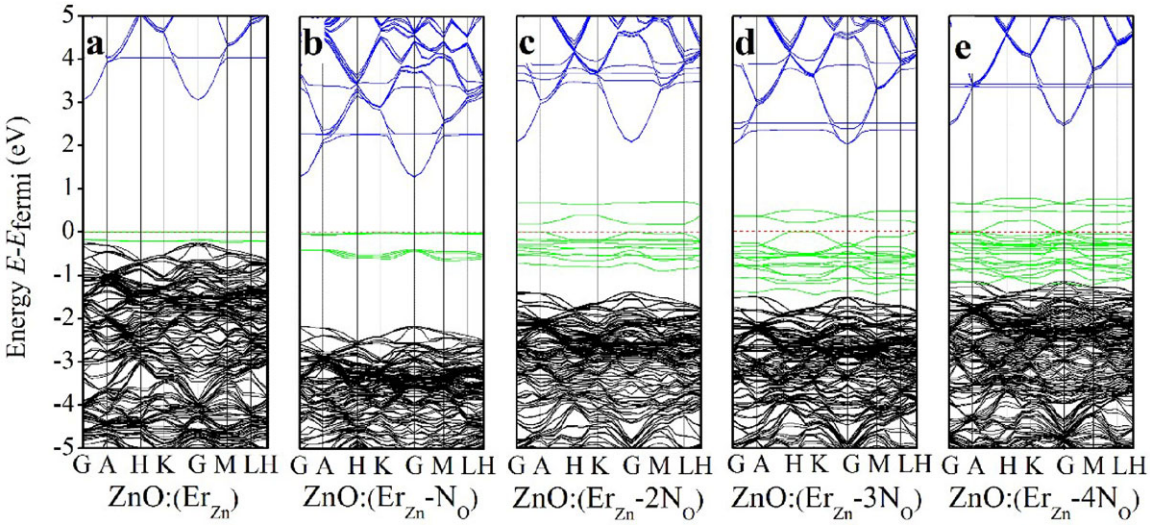

Figure 3. Band structures of ZnO:(Er_{Zn}-mN_O) ($m = 0, 1, 2, 3, 4$) calculated by GGA+U method. The Fermi level is set to zero. An obvious impurity band (green lines) is introduced in the band gap after N atoms are doped into the ZnO:(Er_{Zn}) matrix. With increasing the N concentration, the impurity band gradually expands and finally becomes tail of the valence band.

The defect transition energies became shallower with increasing the N concentration. Under Zn-rich growth conditions, the formation energy increases as the N concentration grows, with the neutral Er_{Zn}-N_O complex approaching the lowest formation energy. However, under the Zn-poor growth environment, the formation energy of the neutral Er_{Zn}-$4N_O$ complex is the highest, and it can be reduced to minimum after the ionization to –3.

2.4. Electronic Properties

The band structures of the ZnO:(Er_{Zn}-mN_O) ($m = 0, 1, 2, 3, 4$) doping systems were calculated referring to the Fermi level at zero, as shown in **Figure 3**. Their corresponding VBM, CBM, and E_g (summarized in Table S2 in the Supporting Information) show that both the VBM and CBM move toward lower energy when N is doped into the ZnO:(Er_{Zn}) system. With increasing the N concentration, nevertheless, both the VBM and CBM move toward higher energy. The band gap E_g also increases with an increase of N atoms in the ZnO:(Er_{Zn}) system, as $E_g = 3.281$, 3.432, 3.470, 3.507, and 3.565 eV, for $m = 0, 1, 2, 3,$ and 4, respectively. Of them, the result of $E_g = 3.281$ at $m = 0$ agrees well with the available experimental value of 3.23 eV.[40] Noticeable impurity bands (green lines) are introduced in the band gap after N atoms are doped into the ZnO:(Er_{Zn}) matrix. With increasing the N concentration, the impurity band gradually expands and finally becomes tail of the valence band. The band-tail states are not good extended states for carriers, thus leading to degradation of the electrical properties of the ZnO:(Er_{Zn}) as a semiconductor.

The total and partial density of states (DOS) of electrons in the ZnO:(Er_{Zn}-mN_O) ($m = 0, 1, 2, 3, 4$) systems (Figure S3 in Supporting Information) manifest that the valence band is composed of the hybridization among the Zn-3*d*, O-2*p*, and Er-4*f* states, and the VBM is mainly attributed to the O-2*p* states. The conduction band is hybridized by the Zn-4*s*, Er-5*p*, and Er-4*f* states, and dominated by Zn-4*s* states. After doping N into the ZnO:(Er_{Zn}) matrix, the Er-4*f* states move to lower energy. The resonance bonding effect of the Zn-3*d* states may weaken the hybridization between the O-2*p* and Zn-3*d* states, thus leading the valence band toward the lower energy. On the other hand, the shift of Zn-4*s*, Er-5*p*, and Er-4*f* states to the lower energy leads to the downward shift of the CBM. In addition, it can be seen that the impurity band introduced by doping N is originated by the N-2*p* states. With further increasing the N concentration, the hybridization between N-2*p* and Zn-3*d* states and the localization of Er-4*f* states are gradually enhanced, but the hybridization between Er-4*f* and Zn-3*d* states weakens, which may be the reason for the VBM moving to higher energy.

3. Discussion

The defect ionization energies of Er_{Zn}-mN_O ($m = 0, 1, 2, 3, 4$) gradually become smaller with increasing the N concentration, which means that the defect ionization energies can be reduced significantly when more N atoms are incorporated into the Er_{Zn}-N_O complex, thus leading to stable *p*-type doping of ZnO. **Figure 4** shows that the ionization energy of ZnO:(Er_{Zn}-$4N_O$) is the lowest in Er-N codoping systems. This means that ZnO:(Er_{Zn}-$4N_O$) is more likely to ionize and reduce the resistivity. Therefore, how to improve the concentration of the Er_{Zn}-$4N_O$ complex in ZnO:(Er_{Zn}-mN_O) systems under the Zn-poor and Er-rich environment is the key to realize excellent *p*-type ZnO films. On the other hand, under Zn-poor conditions, the presence of Zn vacancy will enhance the *p*-type conductivity because it will introduce more holes in the valence band.[41]

The *p*-type of ZnO doping and codoping elements from previous published literature have been summarized in the "Chart of dopants" according to their valent charge and atomic radius (**Figure 5**). It can be seen in Figure 5 that the marks of Er and N are closer to the positions of O and Zn, and they fall on the positions of dopants that have been implemented. This also indicates

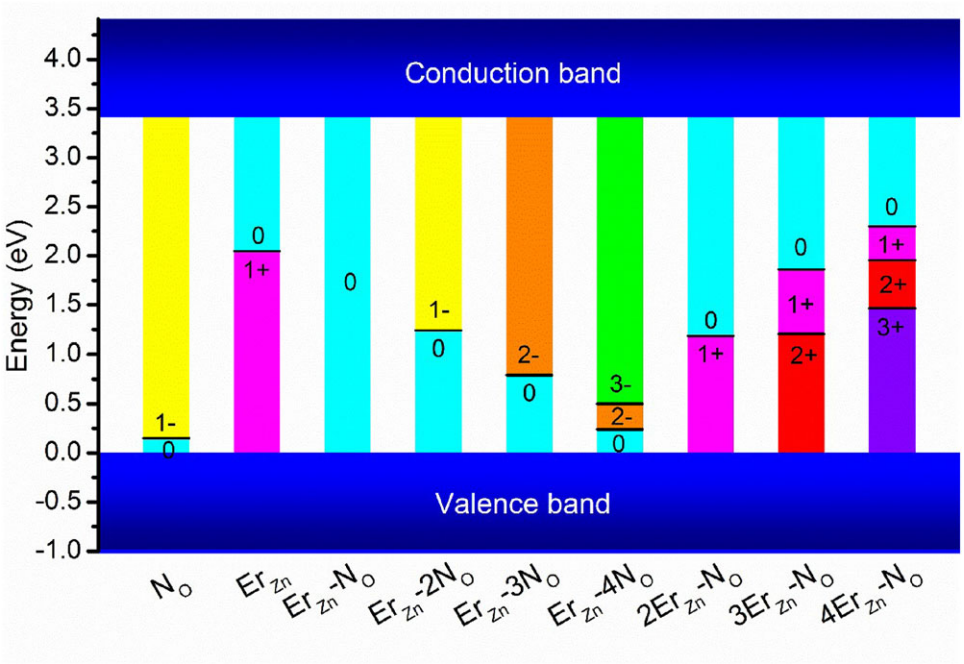

Figure 4. Ionization energies equivalent to the point symbol in Figure 2, alongside the relevant charge states. The ionization energies of nEr_{Zn}-N_O complexes are deeper than those of the Er_{Zn}-mN_O complexes.

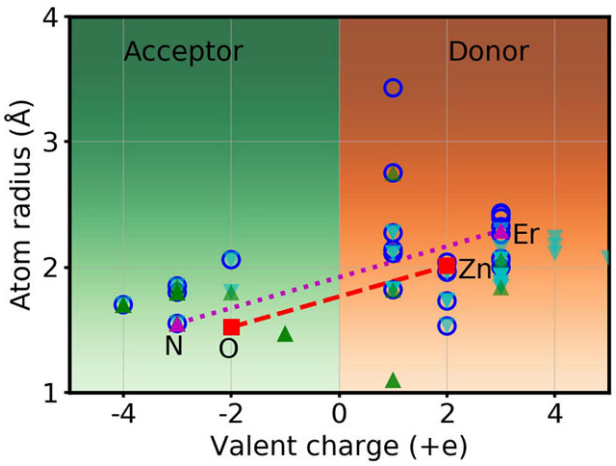

Figure 5. Chart of dopants. Both single dopant and codopants for *p*-type ZnO reported in approximately100 literature are summarized according to their valent charge and atomic radius from periodic element table. The matrix elements Zn and O (red squares) are for reference, compared to Er and N (Magenta triangles) in this study. The element doping and codoping are displayed by circle and filled triangles respectively.

that Er-N codoped ZnO may be feasible experimentally. The doping mechanism of dopants in Figure 5was analyzed based on the available experimental data and theoretical model.[4] For example, Group I doping introduced shallow acceptor state. As for the Group V *p*-type doping, the mechanism is complicated and is different for different elements. Most studies focus on the N-doped ZnO. The drawback of N-doping is the quite limited solubility of N which leads to low hole concentrations and high resistivities. The other thing is that besides the formation of N_O acceptors, the shallow double donors $(N_2)_O$ could be developed and resulted in the *p*-type conduction unstable.[42] The Er-N codoping extends the solubility of N in ZnO and improves the stability of *p*-type ZnO.

4. Conclusion

In summary, structural, electronic, and optical properties of the ZnO:(nEr_{Zn}-mN_O) systems in terms of crystal structures, formation energies, ionization energies, and band structures have been studied systematically by the first-principles method. The obtained results show that the N concentration less influences the crystal structures than that of Er. The ionization energies of ZnO:(Er_{Zn}-mN_O) complexes are shallower than those of ZnO:(nEr_{Zn}-N_O), which makes the Er_{Zn}-mN_O complexes the main configurations in Er-N codoped ZnO systems. When more N atoms are doped to be combined with Er_{Zn} to form larger Er_{Zn}-mN_O complexes, the defect ionization energies can be reduced and favor to form stable *p*-type ZnO:(Er_{Zn}-mN_O) films. The ionization energy of ZnO:(Er_{Zn}-$4N_O$) is the lowest in Er-N codoping systems, and it can realize *p*-type semiconductor material with excellent performance. Our results show that codoping Er-N into the ZnO matrix may be a feasible way to realize stable *p*-type ZnO.

5. Experimental Section

First-Principles Calculations: The exchange-correlation potentials of electron–electron interactions were approximated by the generalized gradient approximation (GGA) with Perdew-Burke-Ernzerhof (PBE) functionals. The interactions between the ion core and its valence electrons were described by ultra-soft pseudopotentials. The configurations of the valence electrons used in the calculations were Zn ($3d^{10}$ $4s^2$), Er ($4f^{12}$ $5s^2$ $5p^6$ $6s^2$),

O ($2s^2$ sp^4), and N ($2s^2p^3$). GGA+U method was used to optimize the system energies to correct the bandgap value of ZnO, where the $U_{p,O}$, $U_{d,Zn}$, and $U_{f,Er}$ values adopted in this work were 7, 10.5 and 6 eV, respectively. The reciprocal space was sampled by a $4 \times 4 \times 3$ Monkhorst-Pack mesh in the irreducible Brillouin zone for the $3 \times 3 \times 2$ supercell. The cutoff energy for the plane wave basis was set to be 510 eV. In the optimization process, the energy variation, maximum tolerances of the force, stress, and atomic displacement were set to be 1.0×10^{-6} eV/atom, 0.03 eV $Å^{-1}$, 0.05 GPa and 0.01 Å, respectively. More details about the model and computations are in the Supporting Information.

Supporting Information

Supporting Information is available from the Wiley Online Library or from the author.

Acknowledgements

This work was financially supported by the National Natural Science Foundation of China Grant Nos. 11464001, 11504060 and 51661003, the Scientific Research Project for Higher Education of Guangxi Zhuang Autonomous Region (Grant No. KY2015ZD006), and the Doctoral Scientific Research Foundation of Guangxi University (Grant No.XBZ160084).

Conflict of Interest

The authors declare no conflict of interest.

Keywords

defect formation energy, Er-N codoping, first principles, *p*-type ZnO

Received: September 10, 2018
Revised: October 21, 2018
Published online: November 16, 2018

[1] A. Tsukazaki, A. Ohtomo, T. Onuma, M. Ohtani, T. Makino, M. Sumiya, K. Ohtani, S. F. Chichibu, S. Fuke, Y. Segawa, H. Ohno, H. Koinuma, M. Kawasaki, *Nat. Mater.* **2005**, *4*, 42.
[2] Z. R. Tian, J. A. Voigt, J. Liu, B. McKenzie, M. J. McDermott, M. A. Rodriguez, *Nat. Mater.* **2003**, *2*, 821.
[3] P. Sharma, A. Gupta, K. V. Rao, F. J. Owens, R. Sharma, R. Ahuja, J. M. Guillen, B. Johansson, G. A. Gehring, *Nat. Mater.* **2003**, *2*, 673.
[4] F. Xiu, J. Xu, P. C. Joshi, C. A. Bridges, M. P. Paranthaman, in *Semiconductor Materials for Solar Photovoltaic Cells* (Eds: M. P. Paranthaman, W. Wong-Ng, R. N. Bhattacharya), Springer, Switzerland **2016**, 105.
[5] M. L. Tu, Y. K. Su, C. Y. Ma, *J. Appl. Phys.* **2006**, *100*, 2208.
[6] Y. J. Zeng, Z. Z. Ye, W. Z. Xu, D. Y. Li, J. G. Lu, L. P. Zhu, B. H. Zhao, *Appl. Phys. Lett.* **2006**, *88*, 3270.
[7] A. Allenic, W. Guo, Y. B. Chen, M. B. Katz, G. Y. Zhao, Y. Che, Z. D. Hu, B. Liu, S. B. Zhang, X. Q. Pan, *Adv. Mater.* **2010**, *19*, 3333.
[8] S. S. Lin, J. G. Lu, Z. Z. Ye, H. P. He, X. Q. Gu, L. X. Chen, J. Y. Huang, B. H. Zhao, *Solid State Commun.* **2008**, *148*, 25.
[9] S. P. Wang, C. X. Shan, B. H. Li, J. Y. Zhang, B. Yao, D. Z. Shen, X. W. Fan, *J. Cryst. Growth* **2009**, *311*, 3577.
[10] M. A. Myers, J. H. Lee, Z. Bi, H. Wang, *J. Phys.: Condens. Matter.* **2012**, *24*, 145802.
[11] T. Yamamoto, H. Katayamayoshida, *Jpn. J. Appl. Phys.* **1999**, *38*, L166.
[12] Y. R. Sui, B. Yao, L. Xiao, L. L. Yang, J. Cao, X. F. Li, G. Z. Xing, J. H. Lang, X. Y. Li, S. Q. Lv, *Appl. Surf. Sci.* **2013**, *287*, 484.
[13] L. Chen, Z. Xiong, Q. Wan, D. Li, *Opt. Mater.* **2010**, *32*, 1216.
[14] D. Li, W. Zhang, X. Yu, Z. Jiang, L. Luan, Y. Chen, D. Li, *Appl. Surf. Sci.* **2012**, *258*, 10064.
[15] W. Li, C. Kong, G. Qin, H. Ruan, L. Fang, *J. Alloys Compd.* **2014**, *609*, 173.
[16] Y. Gai, G. Tang, J. Li, *J. Phys. Chem. Solids* **2011**, *72*, 725.
[17] T. P. Rao, M. C. S. Kumar, *J. Alloys Compd.* **2011**, *509*, 8676.
[18] H. Shen, C. X. Shan, J. S. Liu, B. H. Li, Z. Z. Zhang, D. Z. Shen, *Phys. Status Solidi* **2013**, *250*, 2102.
[19] C. X. Shan, J. S. Liu, Y. J. Lu, B. H. Li, F. C. Ling, D. Z. Shen, *Opt. Lett.* **2015**, *40*, 3041.
[20] Y. R. Sui, B. Yao, Z. Hua, G. Z. Xing, X. M. Huang, T. Yang, L. L. Gao, T. T. Zhao, H. L. Pan, H. Zhu, *J. Phys. D: Appl. Phys.* **2009**, *42*, 065101.
[21] Z. Xiong, L. Chen, C. Zheng, L. Luo, Q. Wan, *Scr. Mater.* **2010**, *63*, 1069.
[22] X. Tang, Y. Deng, D. Wagner, L. Yu, H. Lü, *Solid State Commun.* **2012**, *152*, 1.
[23] E. Przezdziecka, E. Kaminska, K. P. Korona, E. Dynowska, W. Dobrowolski, R. Jakiela, L. Klopotowski, J. Kossut, *Semicond. Sci. Technol.* **2007**, *22*, 10.
[24] L. Cao, L. Zhu, Y. Li, M. Yang, Z. Ye, *Mater. Lett.* **2012**, *86*, 34.
[25] L. Balakrishnan, S. Gowrishankar, J. Elanchezhiyan, N. Gopalakrishnan, *Phys. B* **2011**, *406*, 4447.
[26] N. X. Tian, L. Xiang, L. Zhong, Y. C. Yong, H. S. Cheng, Z. W. Hui, *Appl. Surf. Sci.* **2014**, *316*, 62.
[27] Y. Xu, T. Yang, B. Yao, Y. F. Li, Z. H. Ding, J. C. Li, H. Z. Wang, Z. Z. Zhang, L. G. Zhang, H. F. Zhao, *Ceram. Int.* **2014**, *40*, 2161.
[28] G. Muruganandam, N. Mala, S. Pandiarajan, N. Srinivasan, R. Ramya, E. Sindhuja, K. Ravichandran, *J. Mater. Sci.: Mater. Electron.* **2017**, *28*, 18228.
[29] P. Sharma, R. Bhardwaj, A. Kumar, S. Mukherjee, *J. Phys. D: Appl. Phys.* **2018**, *51*, 015103.
[30] B. Y. Oh, M. C. Jeong, T. H. Moon, W. Lee, J. M. Myoung, J. Y. Hwang, D. S. Seo, *J. Appl. Phys.* **2006**, *99*, 1348.
[31] P. K. Nayak, J. Yang, J. Kim, S. Chung, J. Jeong, C. Lee, Y. Hong, *J. Phys. D: Appl. Phys.* **2009**, *42*, 035102.
[32] X. Zeng, A. Junlin Yuan, L. Zhang, *J. Phys. Chem. C* **2008**, *112*, 3503.
[33] Z. Meng, X. Mo, X. Cheng, Y. Zhou, X. Tao, Y. Ouyang, *Mater. Res. Express* **2017**, *4*, 035903.
[34] Y. Yang, Y. Li, C. Wang, C. Zhu, C. Lv, X. Ma, D. Yang, *Adv. Opt. Mater.* **2014**, *2*, 240.
[35] Y. Liu, C. Xu, Q. Yang, *J. Appl. Phys.* **2009**, *105*, 198.
[36] X. Yu, S. Liang, Z. Sun, Y. Duan, Y. Qin, L. Duan, H. Xia, P. Zhao, D. Li, *Opt. Commun.* **2014**, *313*, 90.
[37] X. L. Xu, Y. Chen, S. Y. Ma, W. Q. Li, Y. Z. Mao, *Sens. Actuators, B* **2015**, *213*, 222.
[38] H. Li, Y. Lv, J. Li, Y. Ke, *J. Alloys Compd.* **2014**, *617*, 102.
[39] R. Peretti, A. M. Jurdyc, B. Jacquier, W. Blanc, B. Dussardier, *Optical Materials* **2011**, *33*, 835.
[40] S. D. Senol, *J. Mater. Sci.: Mater. Electr.* **2016**, *27*, 7767.
[41] M. A. Lahmer, K. Guergouri, *Mater. Sci. Semicond. Process.* **2015**, *39*, 148.
[42] J. L. Lyons, A. Janotti, D. W. Van, G. Chris, *Appl. Phys. Lett.* **2009**, *95*, 252105.

